

Supporting Information

**Metal-Modified C₃N₁ Monolayer Sensors for Battery Instability
Monitoring**

Mingyang Gu ^a, Lin Tao ^{a,*}, Davoud Dastan ^b, Jie Dang ^c,
Timing Fang ^d, and Baigang An ^{a,*}

^a *School of Chemical Engineering, University of Science and Technology
Liaoning, Anshan 114051, China*

^b *Department of Materials Science and Engineering, Cornell University, Ithaca,
New York 14850, United States*

^c *College of Materials Science and Engineering, Chongqing University,
Chongqing 400044, China*

^d *School of Chemistry and Chemical Engineering, Qingdao University,
Qingdao 266071, China*

***Corresponding authors at:** School of Chemical Engineering, University of
Science and Technology Liaoning, Anshan 114051, China

E-mail addresses: taolin@ustl.edu.cn (L. Tao),

E-mail addresses: bgan@ustl.edu.cn (B. An)

Table of Contents

Computational section
Details of thermodynamic calculation
Details of diffusion performance calculation
Figure S1. The energy fluctuations with time process for the <i>ab initio</i> molecular dynamics of Cu/Ag-C ₂ N ₁ monolayer.
Figure S2. Electrostatic potential and work function of (a) the Cu-C ₂ N ₁ and (b) the Ag-C ₂ N ₁ monolayer.
Figure S3. Adsorption structures of C ₂ H ₄ at different sites on the Ag-C ₂ N ₁ .
Figure S4. Adsorption structures of C ₂ H ₆ at different sites on the Ag-C ₂ N ₁ .
Figure S5. Adsorption structures of H ₂ O at different sites on the Ag-C ₂ N ₁ .
Figure S6. Adsorption structures of NH ₃ at different sites on the Ag-C ₂ N ₁ .
Figure S7. Adsorption structures of NO ₂ at different sites on the Ag-C ₂ N ₁ .
Figure S8. Adsorption structures of PF ₅ at different sites on the Ag-C ₂ N ₁ .
Figure S9. Adsorption structures of C ₂ H ₄ at different sites on the Cu-C ₂ N ₁ .
Figure S10. Adsorption structures of PF ₅ at different sites on the Cu-C ₂ N ₁ .
Figure S11. Adsorption structures of C ₂ H ₆ at different sites on the Cu-C ₂ N ₁ .
Figure S12. Adsorption structures of NH ₃ at different sites on the Cu-C ₂ N ₁ .
Figure S13. Adsorption structures of H ₂ O at different sites on the Cu-C ₂ N ₁ .
Figure S14. Adsorption structures of NO ₂ at different sites on the Cu-C ₂ N ₁ .
Figure S15. The initial adsorption configuration of gases (PF ₅ , NO ₂ , NH ₃ , H ₂ O, C ₂ H ₄ , and C ₂ H ₆) on the Ag-C ₂ N ₁ .
Figure S16. The initial adsorption configuration of gases (PF ₅ , NO ₂ , NH ₃ , H ₂ O, C ₂ H ₄ , and C ₂ H ₆) on the Cu-C ₂ N ₁ .
Figure S17. The COHP between gases (C ₂ H ₄ , PF ₅ , C ₂ H ₆ , H ₂ O, NH ₃ , and NO ₂) and the Ag-C ₂ N ₁ .
Figure S18. The COHP between gases (C ₂ H ₄ , PF ₅ , C ₂ H ₆ , H ₂ O, NH ₃ , and NO ₂) and the Cu-C ₂ N ₁ .
Figure S19. DOS and PDOS of (a) C ₂ H ₄ , (b) C ₂ H ₆ , (c) PF ₅ , (d) H ₂ O, (e) NH ₃ , (f) NO ₂ on the Ag-C ₂ N ₁ monolayer.
Figure S20. DOS and PDOS of (a) C ₂ H ₄ , (b) C ₂ H ₆ , (c) PF ₅ , (d) H ₂ O, (e) NH ₃ , (f) NO ₂ on the Cu-C ₂ N ₁ monolayer.
Figure S21. The initial and the final stable configurations of gas on the Ag-C ₂ N ₁ . (a) NH ₃ , (b) H ₂ O, (c) PF ₅ , (d) C ₂ H ₆ , (e) C ₂ H ₄ , and (f) NO ₂ .
Figure S22. The initial and the final stable configurations of gas on the Cu-C ₂ N ₁ . (a) NH ₃ , (b) H ₂ O, (c) PF ₅ , (d) C ₂ H ₆ , (e) C ₂ H ₄ , and (f) NO ₂ .
Figure S23. The stable configurations of NO ₂ on the Ag-C ₂ N ₁ at different

temperatures. (a) 300 K, (b) 400 K, (c) 500 K, (d) 600 K, and (e) 700 K.
Figure S24. The stable configurations of NO ₂ on the Cu-C ₂ N ₁ at different temperatures. (a) 300 K, (b) 400 K, (c) 500 K, (d) 600 K, (e) 700 K, and (f) 800 K.
Table S1. The amount of charge transferred by the gas adsorbed.
Table S2. Diffusion coefficient of six gases on the Cu/Ag-C ₂ N ₁ monolayer at 300 K
Table S3. Diffusion coefficients of NO ₂ on the Cu/Ag-C ₂ N ₁ at different temperatures.
Table S4. The recovery time (s) of the gas on the Cu-C ₂ N ₁ .
Table S5. The recovery time (s) of the gas on the Ag-C ₂ N ₁ .
References

Computational section

For the original C₃N₁, Ag-C₂N₁, Cu-C₂N₁, PF₅, NO₂, NH₃, H₂O, C₂H₄, and C₂H₆, all structural optimization and electronic performance calculations are performed using DFT, based on Dmol³ code [1] under the Perdew-Burke-Ernzerhof functional, gradient approximation method correlation [2, 3], double precision number basis set polarization function is used to process atomic orbitals. The dispersion-corrected DFT method was selected based on Grimme vdW correction [4], which can accurately describe the interaction in all weak calculations. The global cut-off radius of real space is 4.9 Å, and the Monkhorst–Pack scheme is used to sample 3 × 2 × 1 k points in the Brillouin area to complete high-quality theoretical evaluation. In addition, the convergence tolerance of geometry optimization is 1 × 10⁻⁵ Ha for the total energy, 0.002 Ha/Å for the atomic force, and 0.005 Å for the highest displacement, respectively. The electron distribution and charge transfer were calculated using the Mulliken method [5]. To eliminate interactions between periodic images, use a 20 Å vacuum layer vertically to the Cu/Ag-C₂N₁ monolayer. The C-N bond length is 1.41 Å, the C-C bond length is 1.43 Å, and the maximum spacing of C-N-C-C is 2.83 Å in the initial C₃N₁ monolayer.

Details of thermodynamic calculation

These mainly include enthalpy, entropy, and the Gibbs free energy.

First, enthalpy (H) is calculated by

$$\begin{aligned}
 H &= H_{trans} + H_{rot} + H_{vib} + RT \\
 &= \frac{R}{2k} \sum_i hv_i + \frac{R}{k} \sum_i \frac{hv_i \exp(-hv_i/kT)}{[1 - \exp(-hv_i/kT)]^2} + 4R
 \end{aligned} \quad (1)$$

where H_{trans} , H_{rot} and H_{vib} are the translation enthalpy, rotation enthalpy, and vibration enthalpy (kcal/mol), respectively. R and T are the ideal gas constant (8.314 J/mol/K) and the absolute temperature (K), accordingly. k is the Boltzmann constant, h is Planck's constant, and ν_i is the vibrational frequency.

Second, entropy (S) is given by

$$\begin{aligned}
 S &= S_{trans} + S_{rot} + S_{vib} \\
 &= \frac{5}{2}R \ln T + \frac{5}{2}R \ln w - \frac{5}{2}R \ln p - 2.3482 \\
 &\quad + \frac{R}{2} \ln \left[\frac{\pi}{\sqrt{\sigma}} \frac{8\pi^2 c l_A}{h} \frac{8\pi^2 c l_B}{h} \frac{8\pi^2 c l_C}{h} \left(\frac{kT}{hc} \right)^3 \right] \\
 &\quad + \frac{3}{2}R + R \sum_i \frac{hv_i/kT \exp(-hv_i/kT)}{1 - \exp(-hv_i/kT)} \\
 &\quad - R \sum_i \ln [1 - \exp(-hv_i/kT)]
 \end{aligned} \quad (2)$$

Where S_{trans} , S_{rot} , and S_{vib} are the translation, rotation, and vibration entropies (cal/mol/K), accordingly. w is the molecular mass, p is the pressure, σ is the symmetry number, c is the molar concentration of the molecules, and $I_{A(B,C)}$ is the moment of inertia.

Finally, the Gibbs free energy (G) (kJ/mol) is defined as

$$G = E(OK) + H - T \cdot S \quad (3)$$

where $E(0 K)$ is the zero-point energy (kcal/mol).



Details of diffusion performance calculation

From the point of view of gas motion (diffusion), the main energy barrier to be overcome in NO₂ adsorption on the Ag-C₂N₁ and Cu-C₂N₁ monolayer was the gas diffusion energy barrier. The diffusion activation energy can be obtained by calculating the gas motion parameters according to molecular dynamics simulation with our previous work [6], and by this means, the energy barrier of NO₂ adsorption on the Cu/Ag-C₂N₁ monolayer can be well verified. Therefore, the mean-squared displacement (MSD) and diffusion coefficients (Ds) were used to investigate the diffusion properties of gases according to the Einstein diffusion law; these quantities were computed by the following equations.

$$MSD(t) = \frac{1}{N} \sum_{i=1}^N \langle [r_i(t) - r_i(0)]^2 \rangle \quad (4)$$

$$D_s = \frac{1}{6} \lim_{t \rightarrow \infty} \frac{d}{dt} \sum_i^n \langle [r_i(t) - r_i(0)]^2 \rangle \quad (5)$$

where N is the number of molecules, $r_i(t)$ is the position of molecule when the time is t , and $r_i(0)$ is the initial position. According to Equations (4) and (5), the diffusion coefficients were calculated and are shown in **Table S2 and S3**.

After a series of the diffusion coefficients, D_s , of NO₂ at different temperatures were obtained, the diffusion activation energy of NO₂ could be calculated by means of the Arrhenius equation:

$$D_s = D_0 \exp(-E'_a / RT) \quad (6)$$

where E'_a , A , and R refer to the Arrhenius activation energy, the Arrhenius factor, and gas constant, respectively. Equation (6) can also be expressed as:

$$\ln D_s = \ln A - E'_a / RT \quad (7)$$

According to the data in **Table S3** and Equation (7), the diffusion activation energy

E'_a could be directly calculated from the slope of the fitted curve. **Figure 6** shows the Arrhenius temperature dependence of the diffusion coefficients along with the activation energy for diffusion. Therefore, the energy barriers to be overcome in the process of NO₂ diffusion to the monolayer of Ag-C₂N₁ and Cu-C₂N₁ are 2.7 kJ/mol and 2.5 kJ/mol.

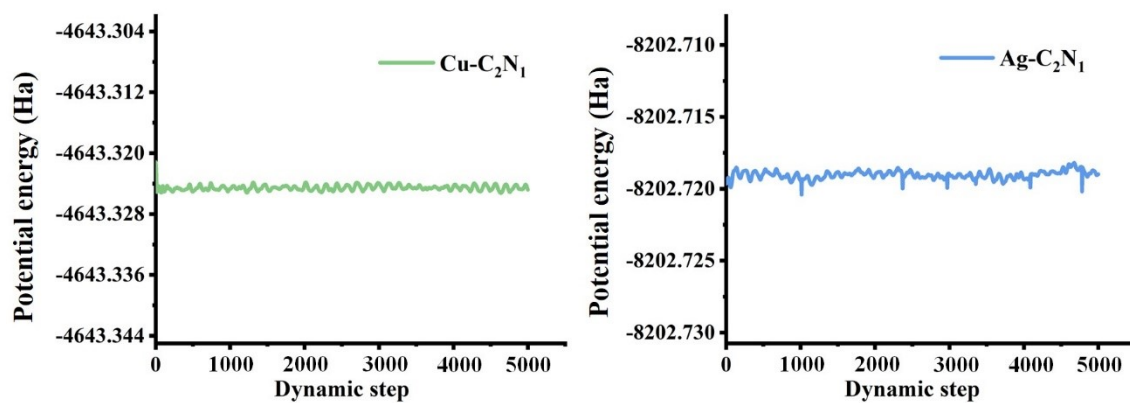


Figure S1. The energy fluctuations with time process for the *ab initio* molecular dynamics of Cu/Ag-C₂N₁ monolayer.

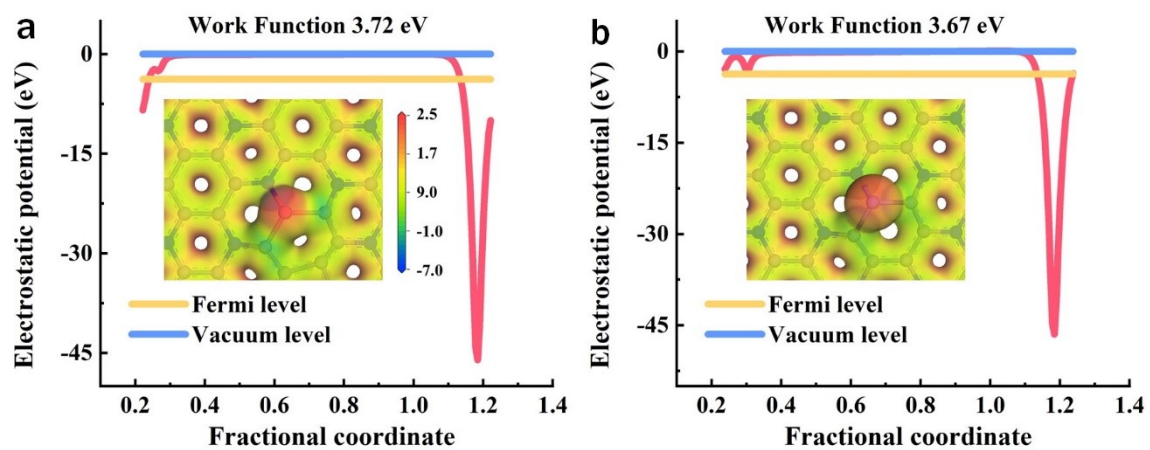


Figure S2. Electrostatic potential and work function of (a) the Cu-C₂N₁ and (b) the Ag-C₂N₁ monolayer.

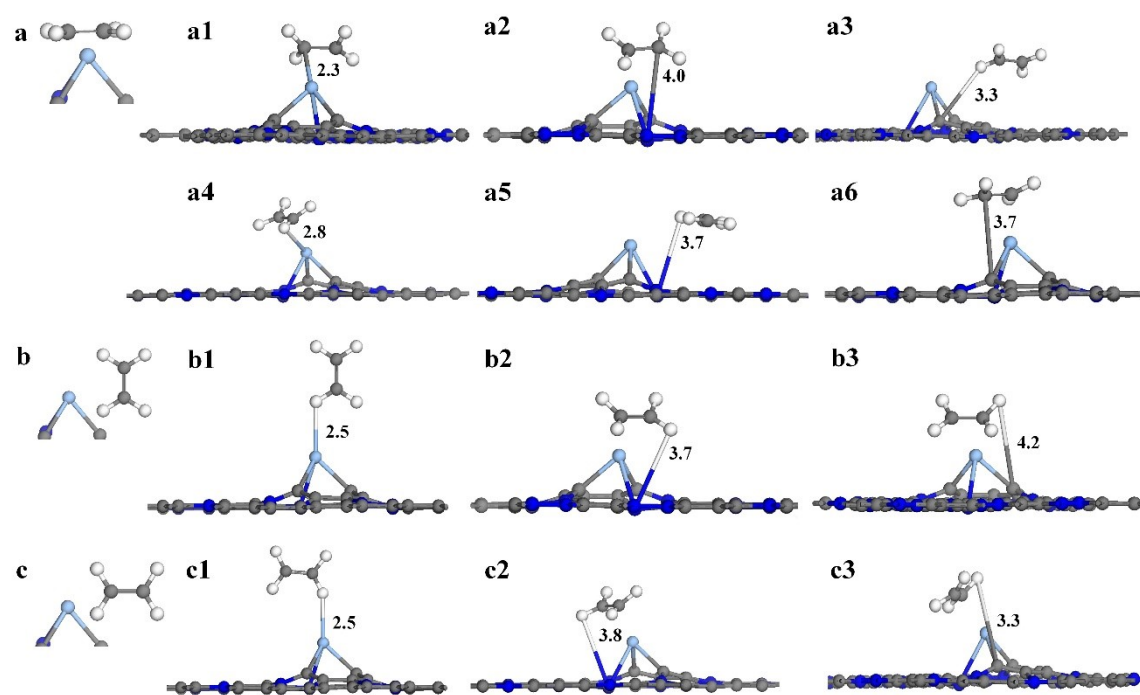


Figure S3. Adsorption structures of C_2H_4 at different sites on the $Ag-C_2N_1$.

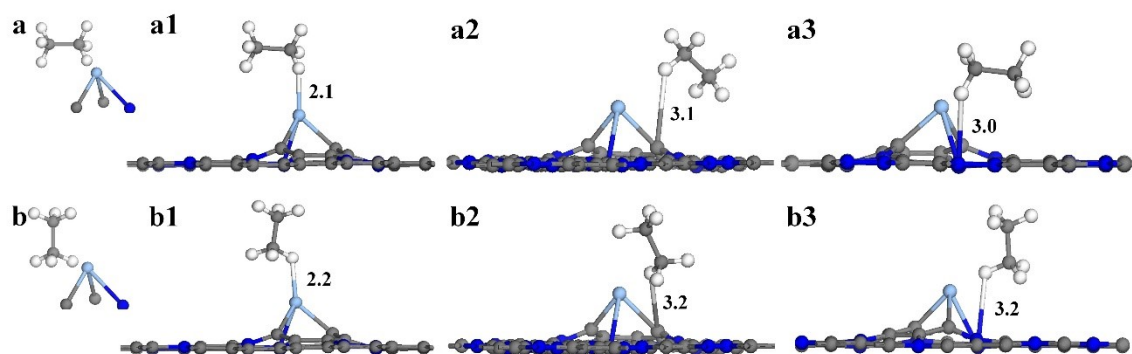


Figure S4. Adsorption structures of C_2H_6 at different sites on the $Ag-C_2N_1$.

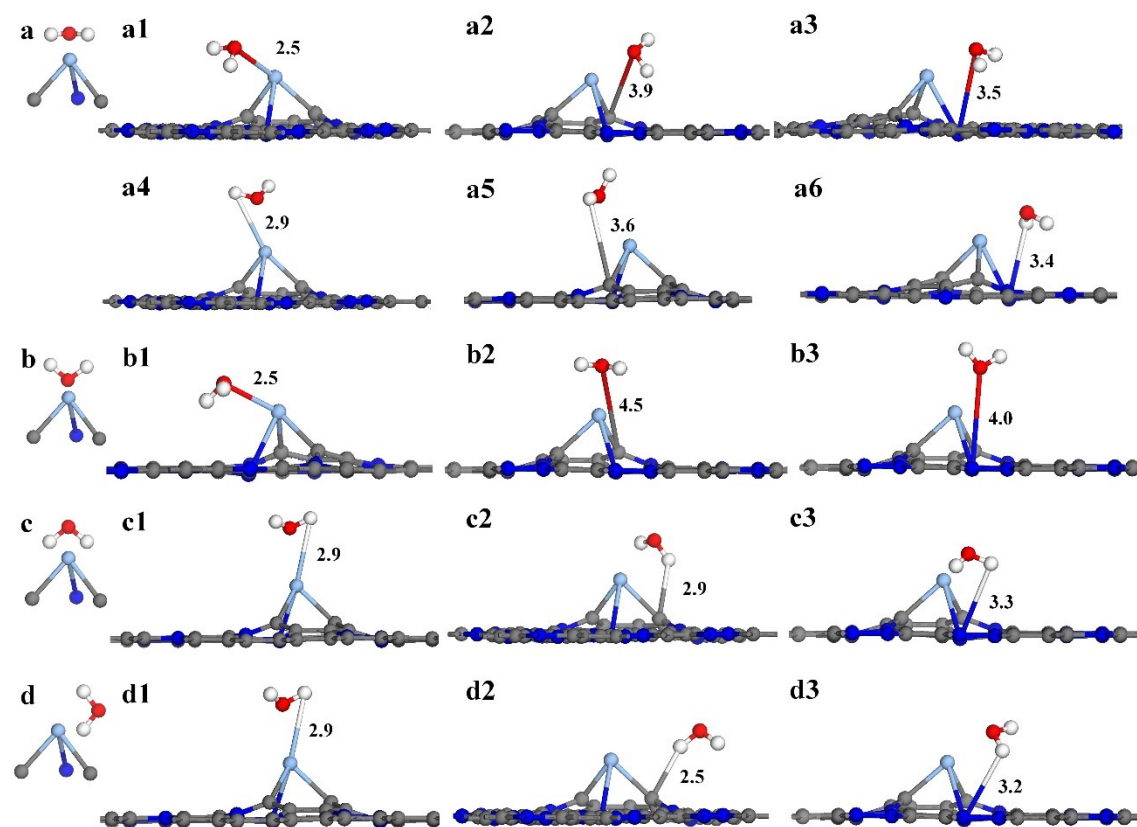


Figure S5. Adsorption structures of H₂O at different sites on the Ag-C₂N₁.

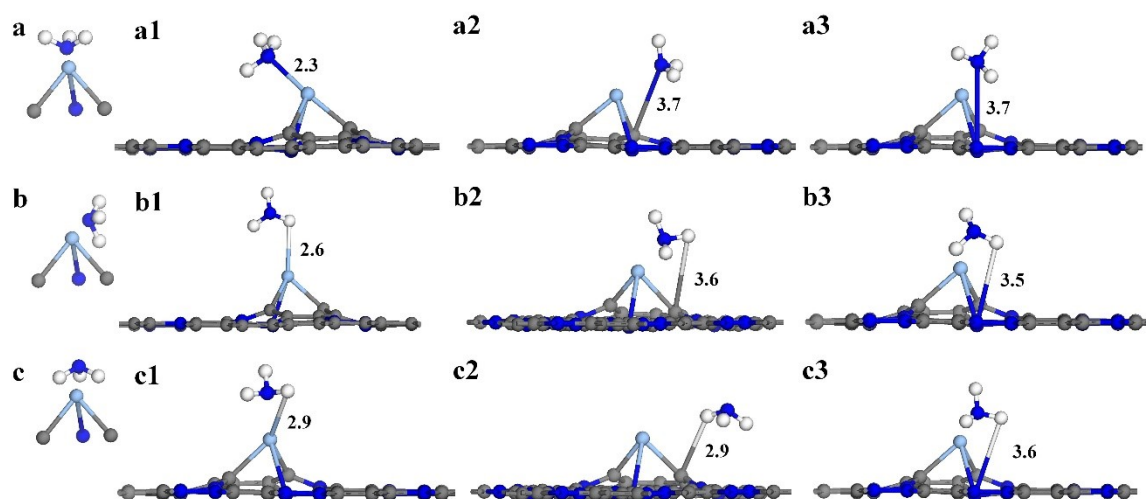


Figure S6. Adsorption structures of NH_3 at different sites on the $\text{Ag-C}_2\text{N}_1$.

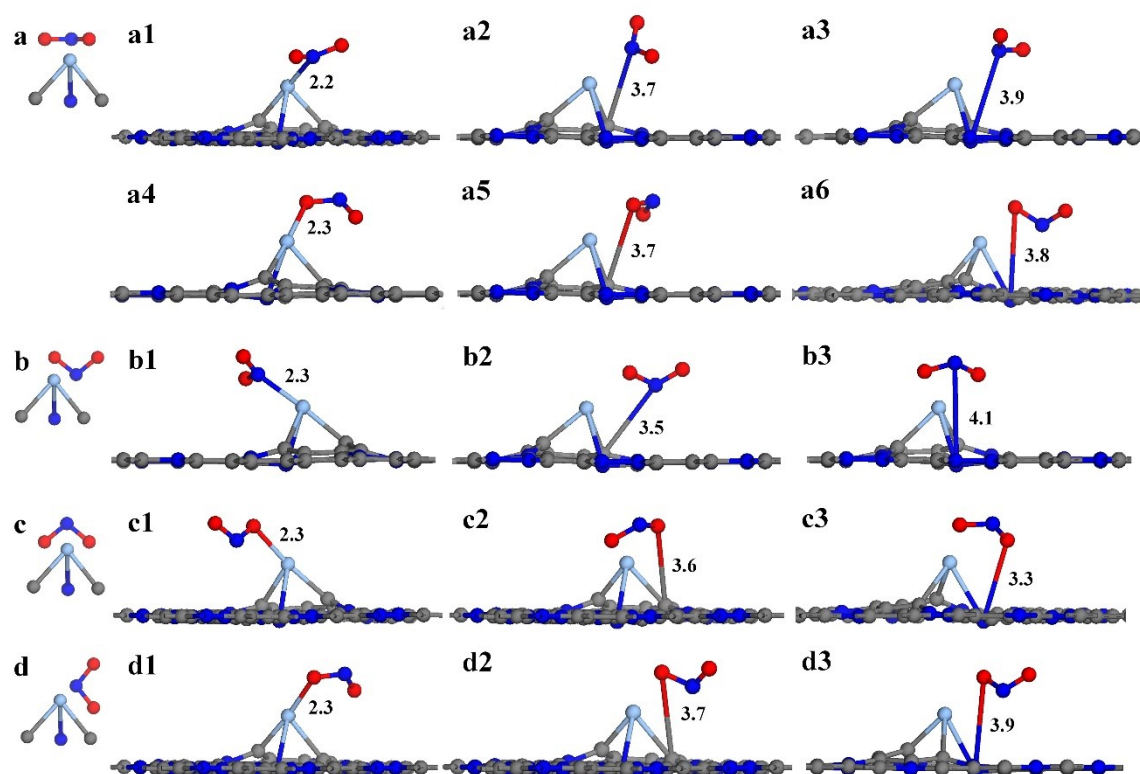


Figure S7. Adsorption structures of NO_2 at different sites on the $\text{Ag-C}_2\text{N}_1$.

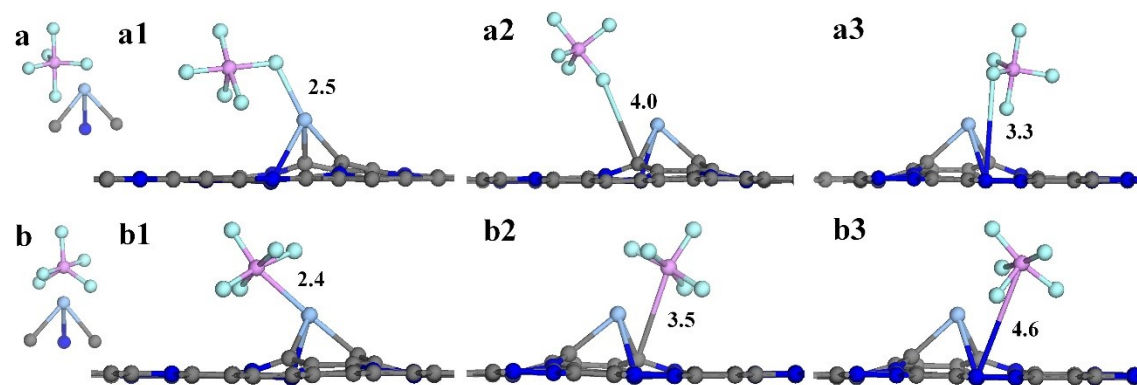


Figure S8. Adsorption structures of PF₅ at different sites on the Ag-C₂N₁.

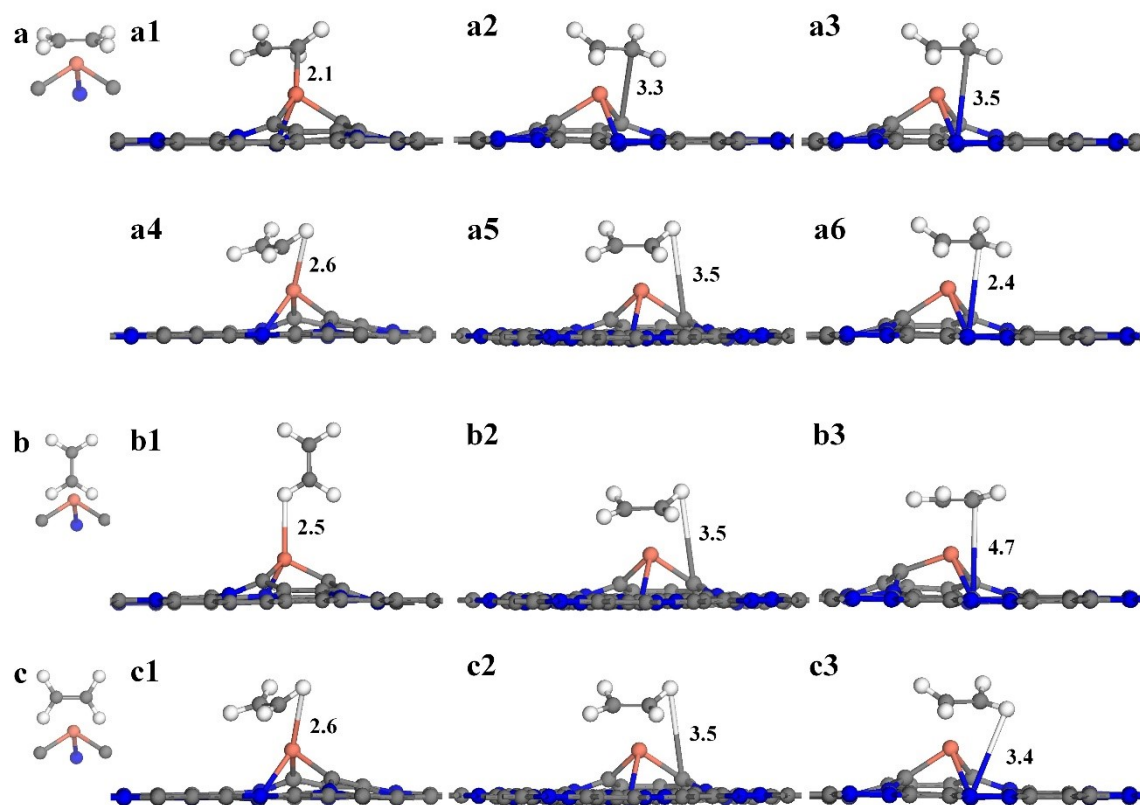


Figure S9. Adsorption structures of C_2H_4 at different sites on the $Cu-C_2N_1$.

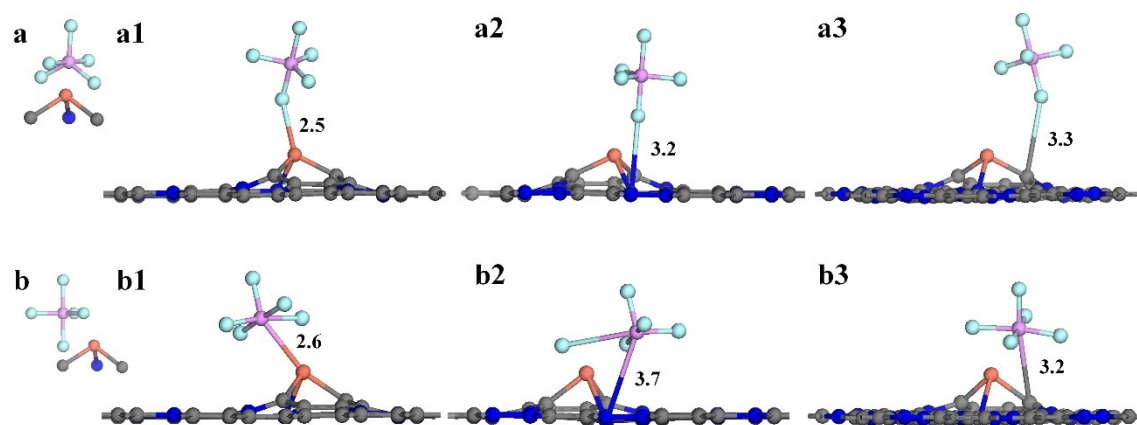


Figure S10. Adsorption structures of PF_5 at different sites on the $\text{Cu-C}_2\text{N}_1$.

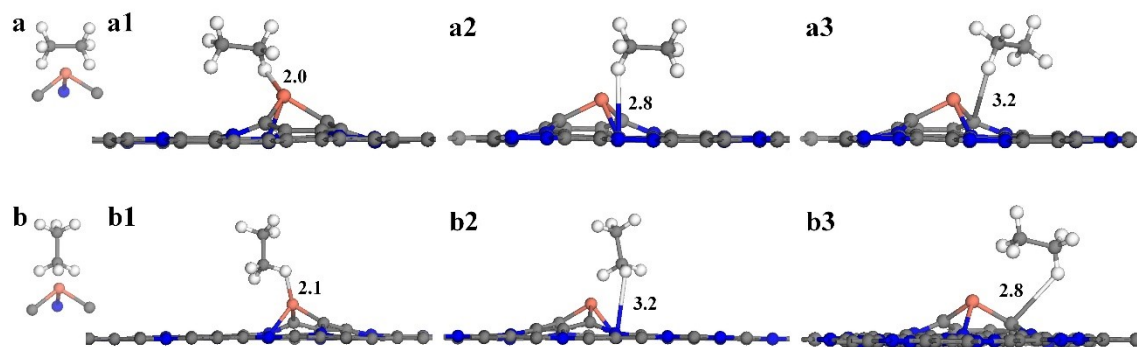


Figure S11. Adsorption structures of C_2H_6 at different sites on the $Cu-C_2N_1$.

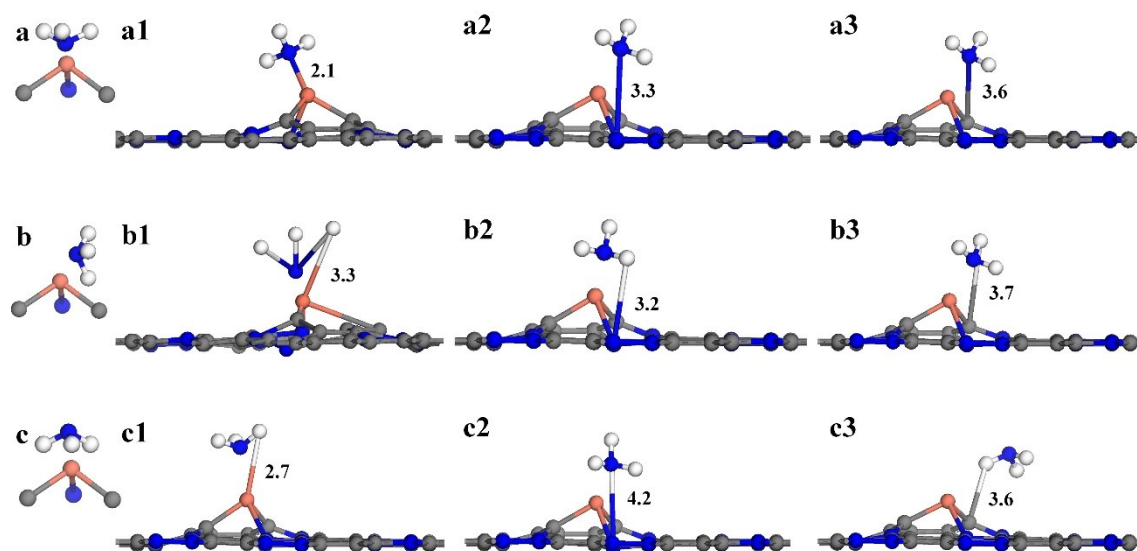


Figure S12. Adsorption structures of NH_3 at different sites on the $\text{Cu-C}_2\text{N}_1$.

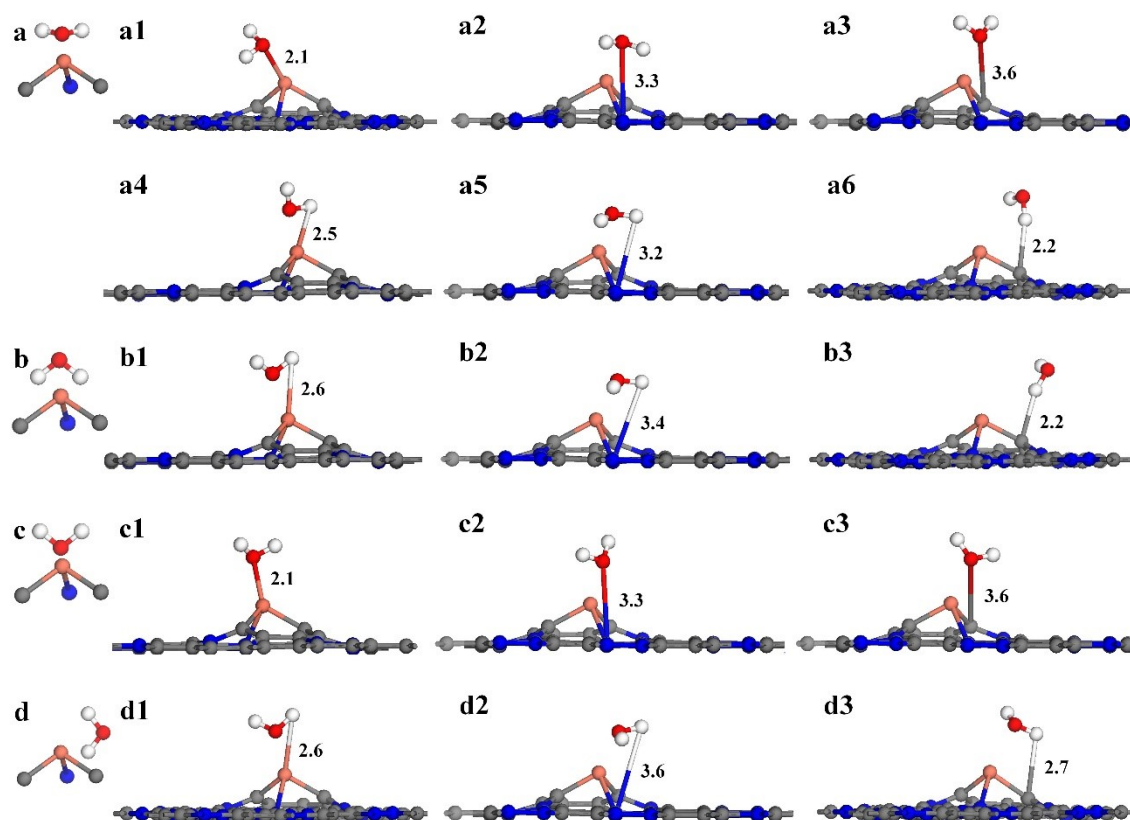


Figure S13. Adsorption structures of H₂O at different sites on the Cu-C₂N₁.

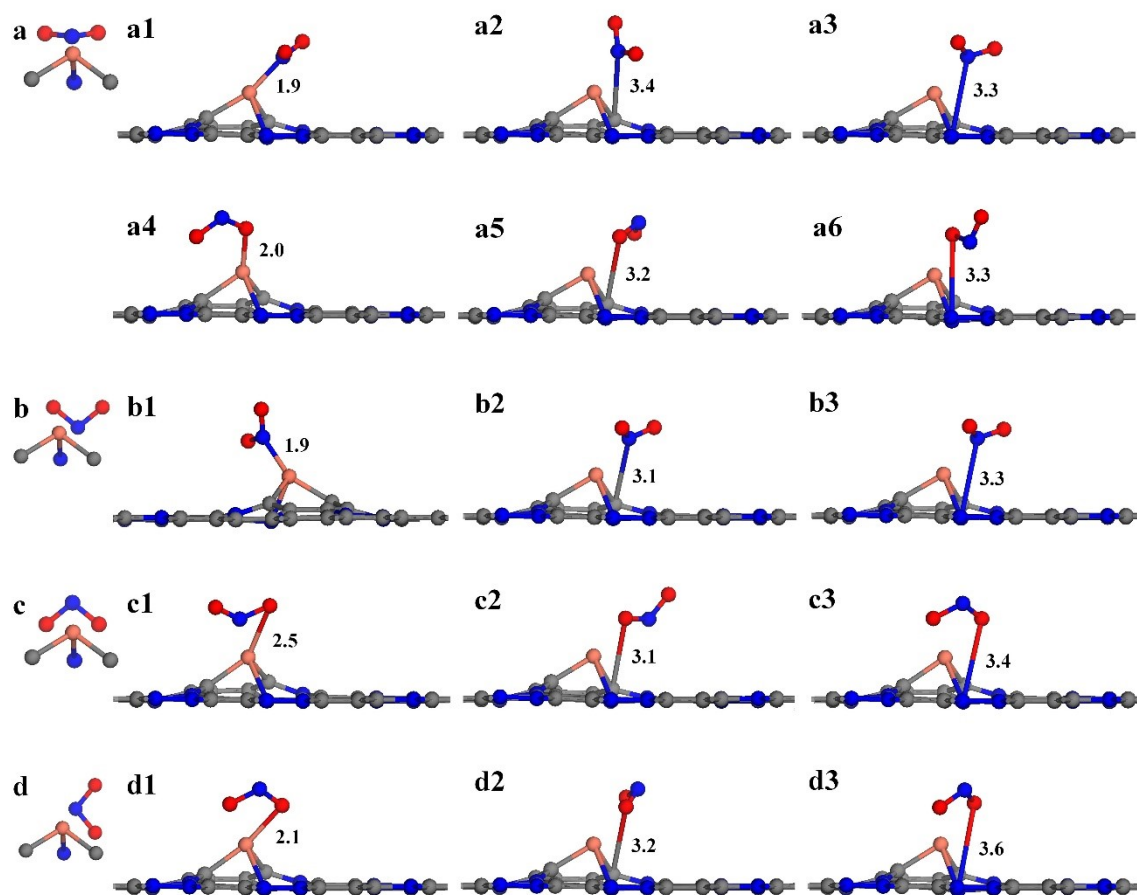


Figure S14. Adsorption structures of NO_2 at different sites on the $\text{Cu-C}_2\text{N}_1$.

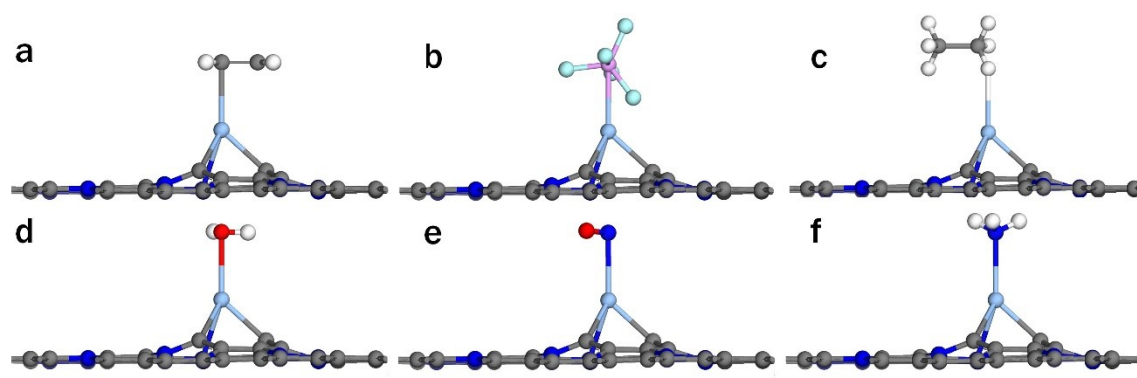


Figure S15. The initial adsorption configuration of gases (PF_5 , NO_2 , NH_3 , H_2O , C_2H_4 , and C_2H_6) on the $\text{Ag-C}_2\text{N}_1$.

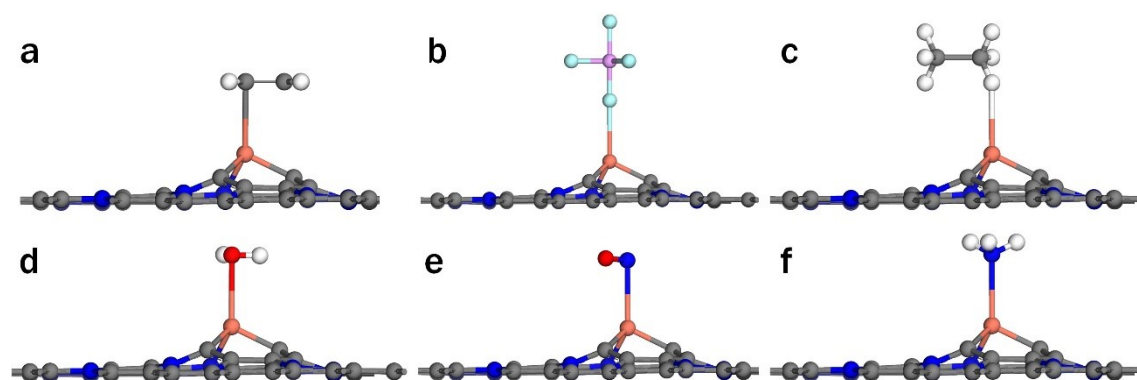


Figure S16. The initial adsorption configuration of gases (PF_5 , NO_2 , NH_3 , H_2O , C_2H_4 , and C_2H_6) on the $\text{Cu-C}_2\text{N}_1$.

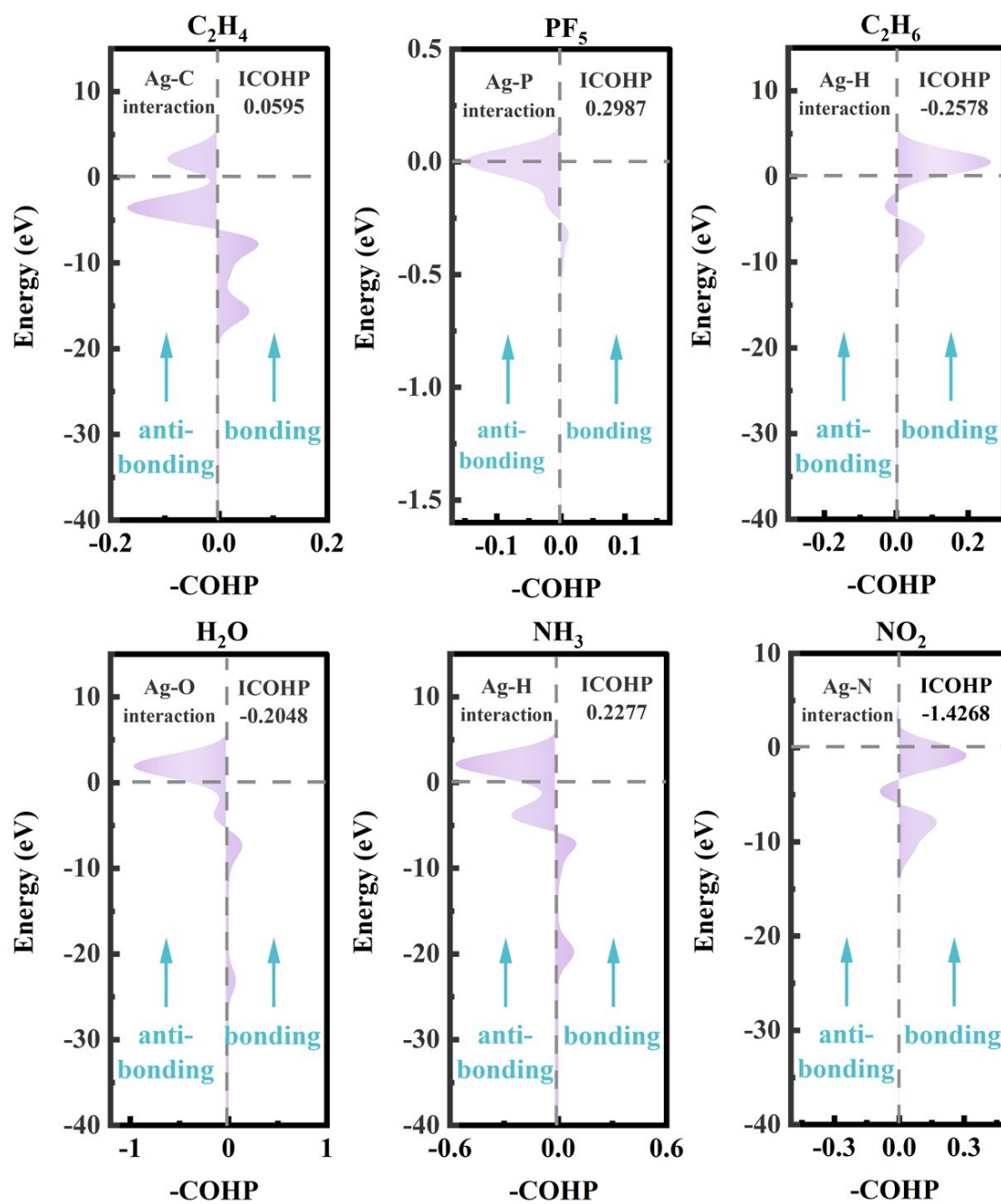


Figure S17. The COHP between gases (C₂H₄, PF₅, C₂H₆, H₂O, NH₃, and NO₂) and the Ag-C₂N₁.

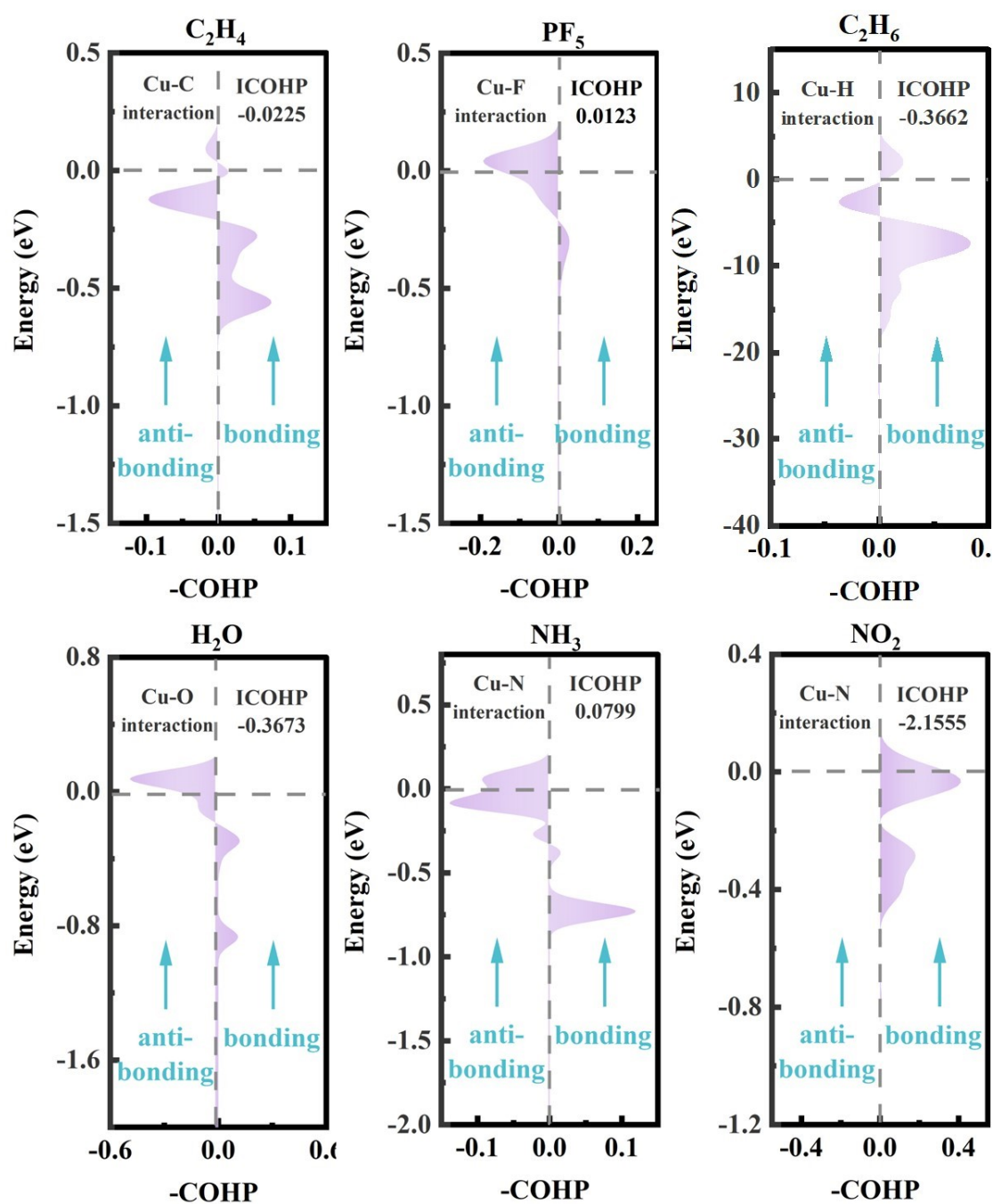


Figure S18. The COHP between gases (C₂H₄, PF₅, C₂H₆, H₂O, NH₃, and NO₂) and the Cu-C₂N₁.

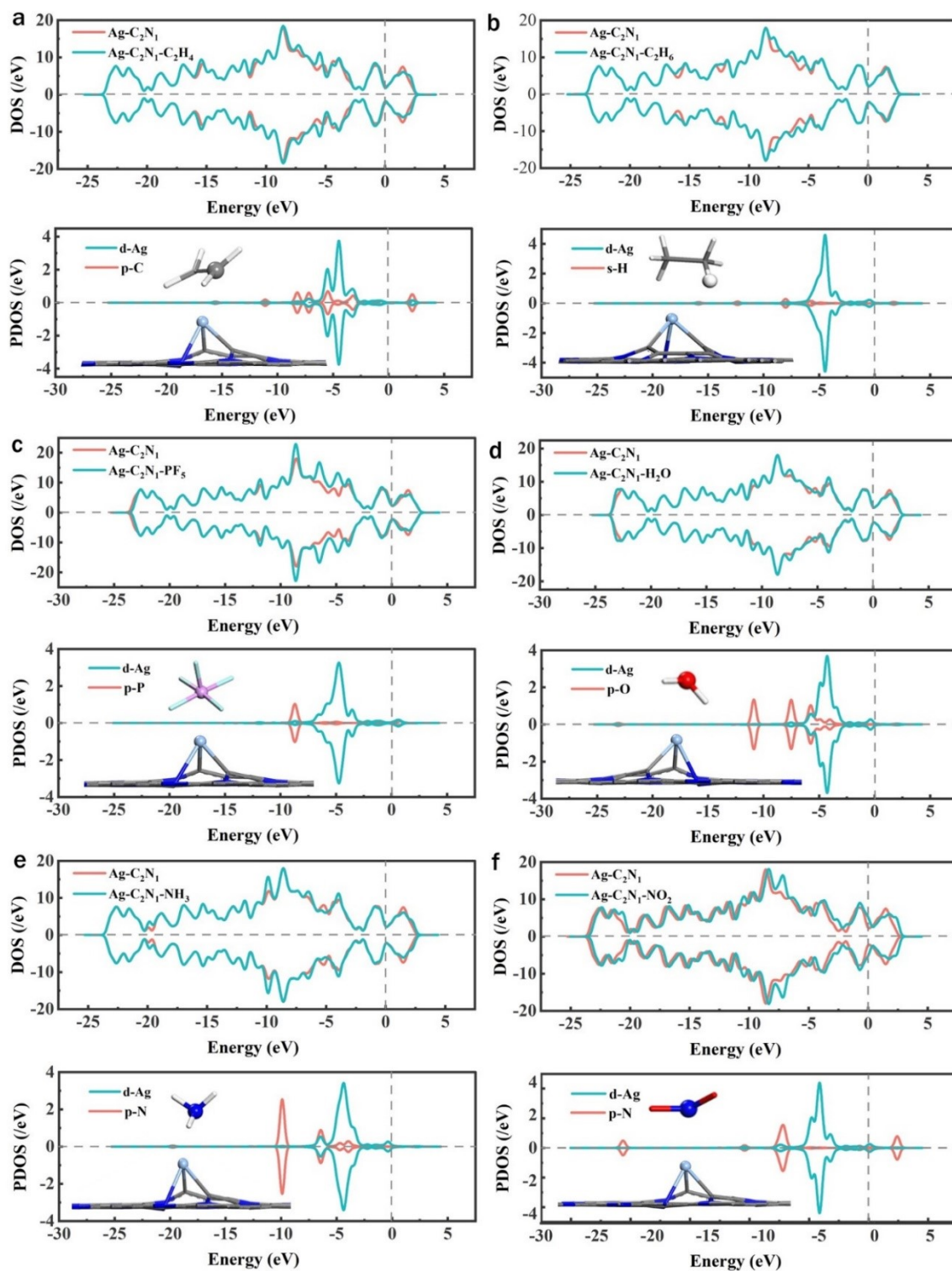


Figure S19. DOS and PDOS of (a) C₂H₄, (b) C₂H₆, (c) PF₅, (d) H₂O, (e) NH₃, (f) NO₂ on the Ag-C₂N₁ monolayer.

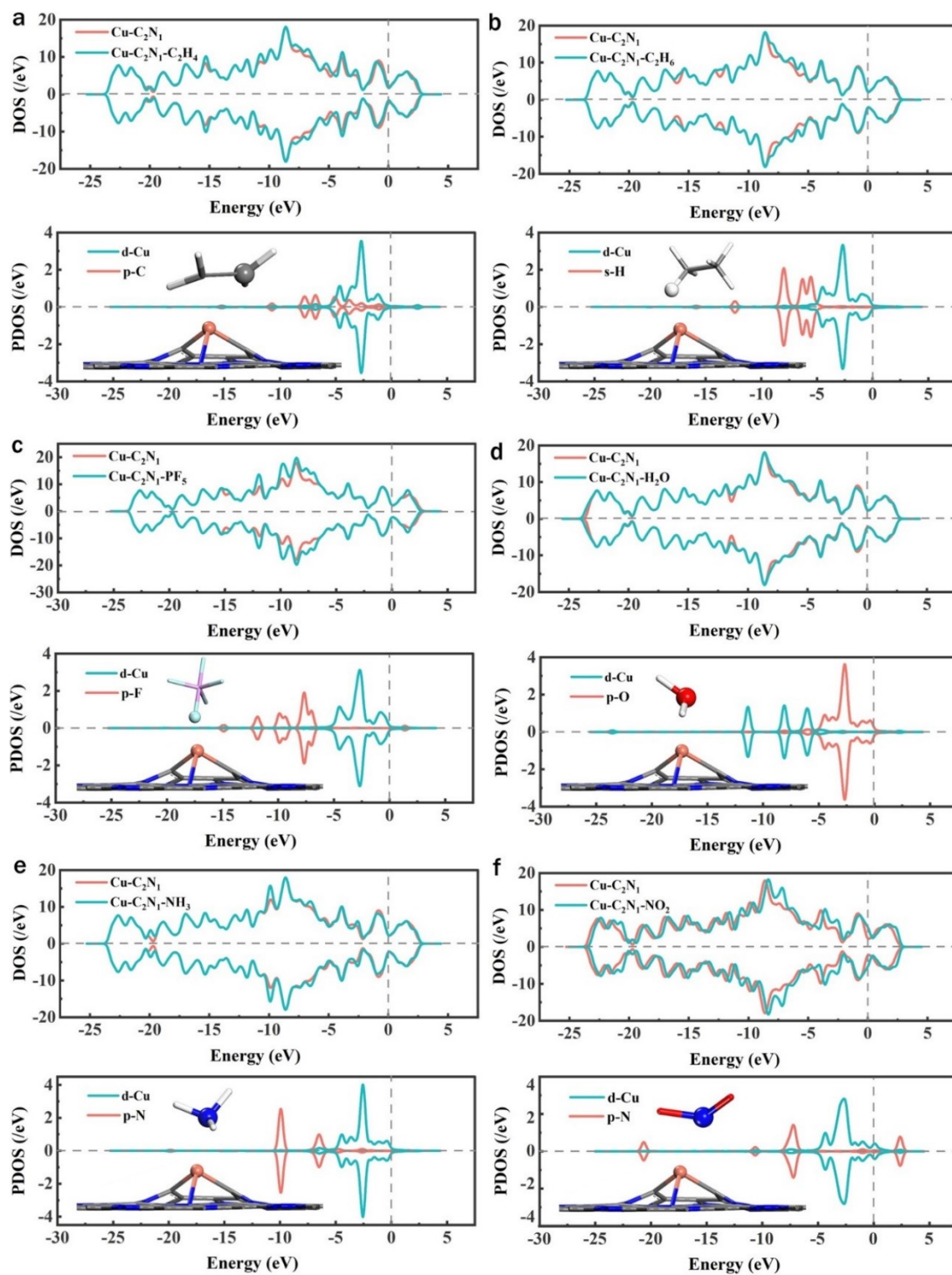


Figure S20. DOS and PDOS of (a) C₂H₄, (b) C₂H₆, (c) PF₅, (d) H₂O, (e) NH₃, (f) NO₂ on the Cu C₂N₁ monolayer.

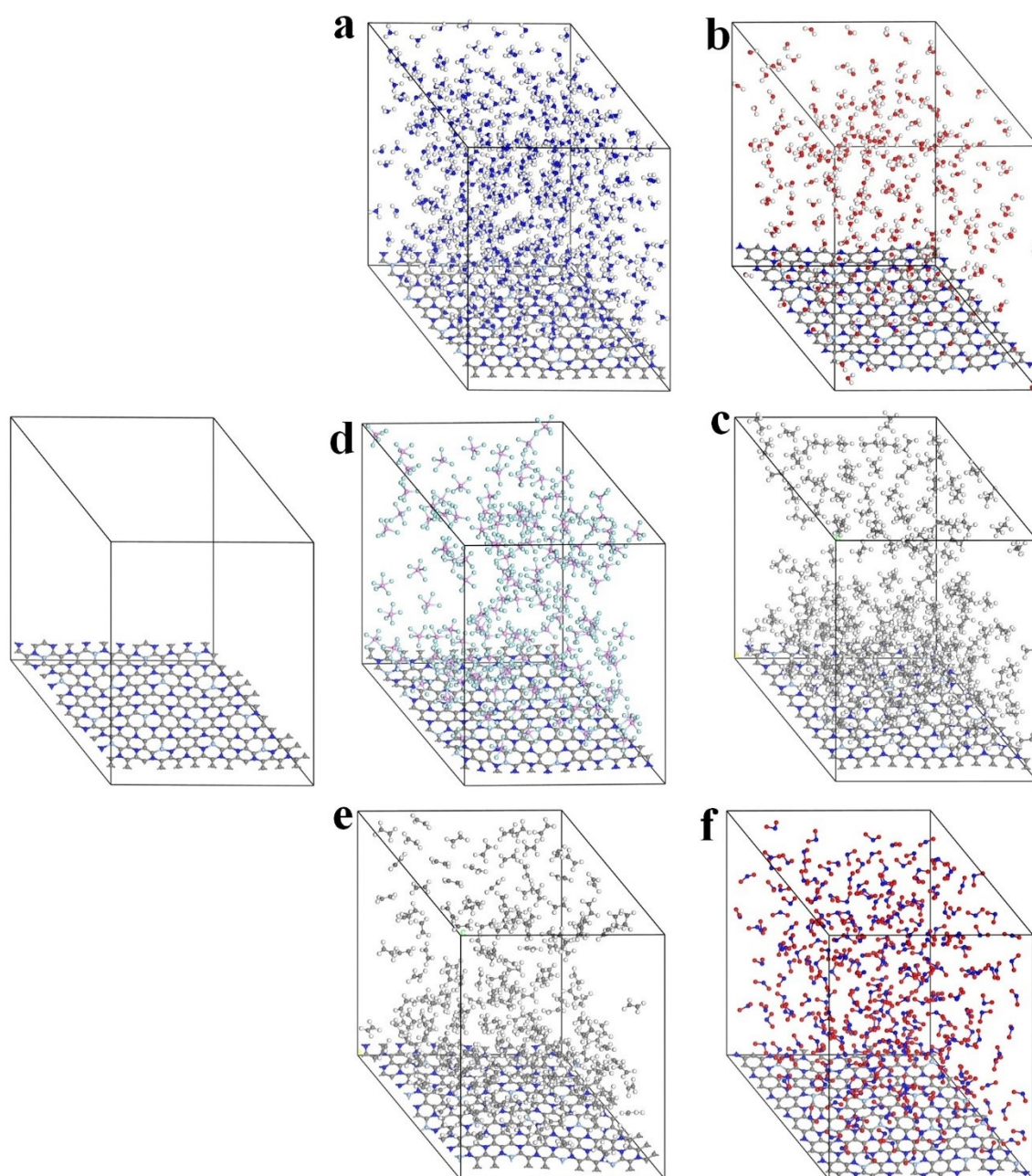


Figure S21. The initial and the final stable configurations of gas on the Ag-C₂N₁. (a) NH₃, (b) H₂O, (c) PF₅, (d) C₂H₆, (e) C₂H₄, and (f) NO₂.

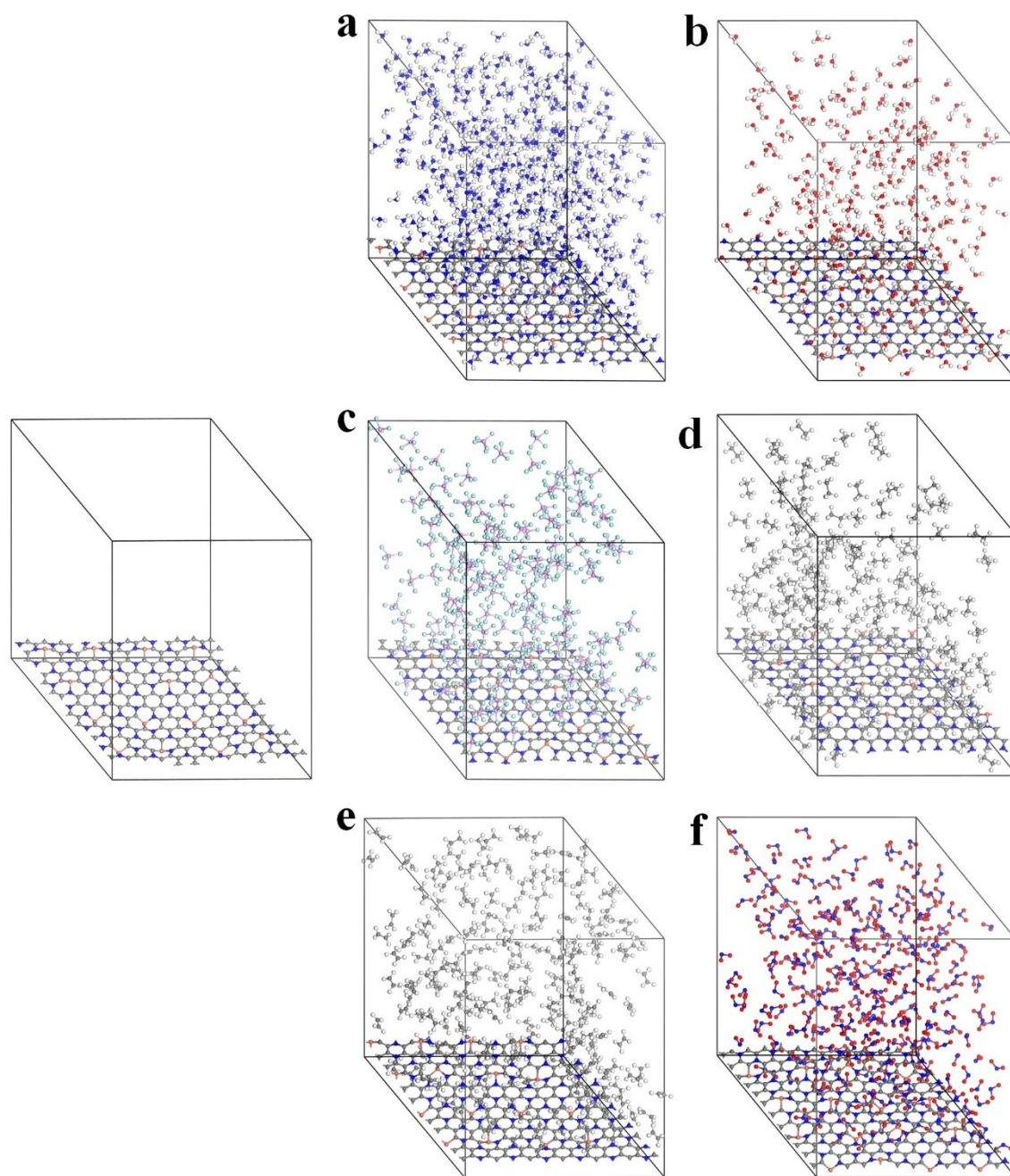


Figure S22. The initial and the final stable configurations of gas on the Cu-C₂N₁. (a) NH₃, (b) H₂O, (c) PF₅, (d) C₂H₆, (e) C₂H₄, and (f) NO₂.

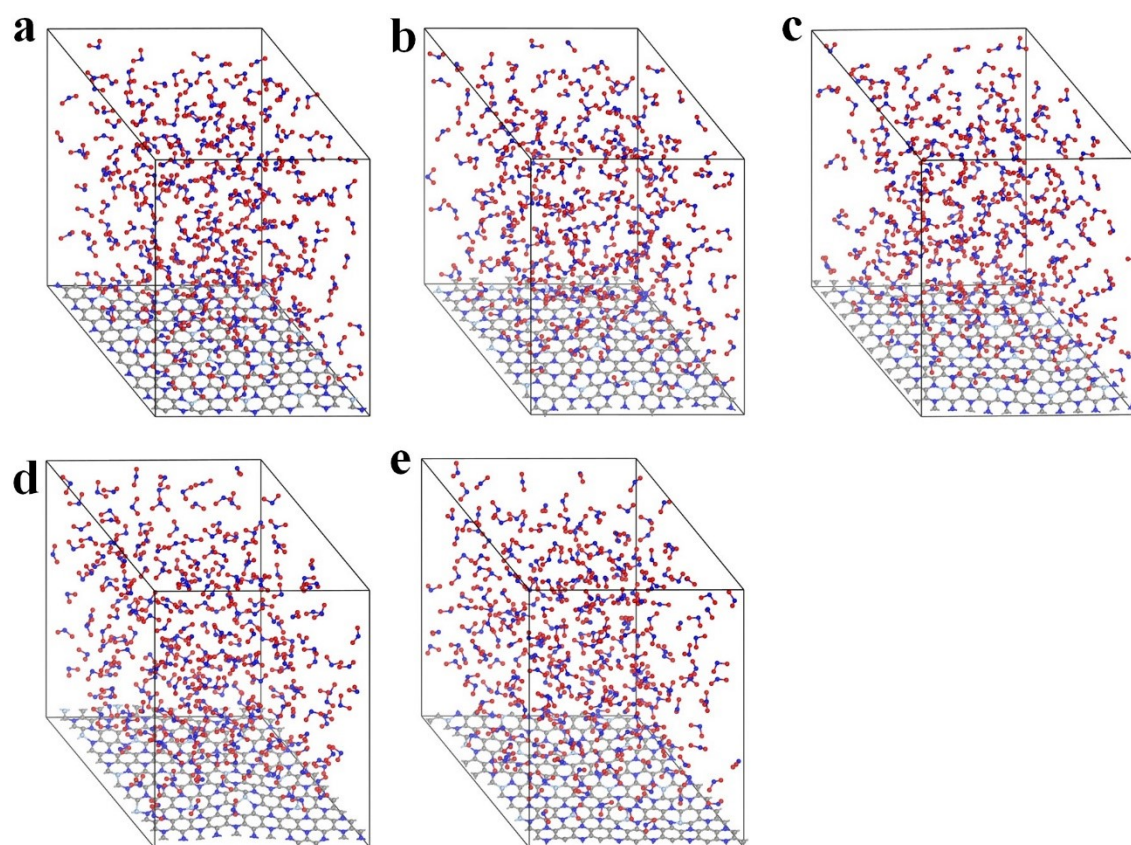


Figure S23. The stable configurations of NO₂ on the Ag-C₂N₁ at different temperatures. (a) 300 K, (b) 400 K, (c) 500 K, (d) 600 K, and (e) 700 K.

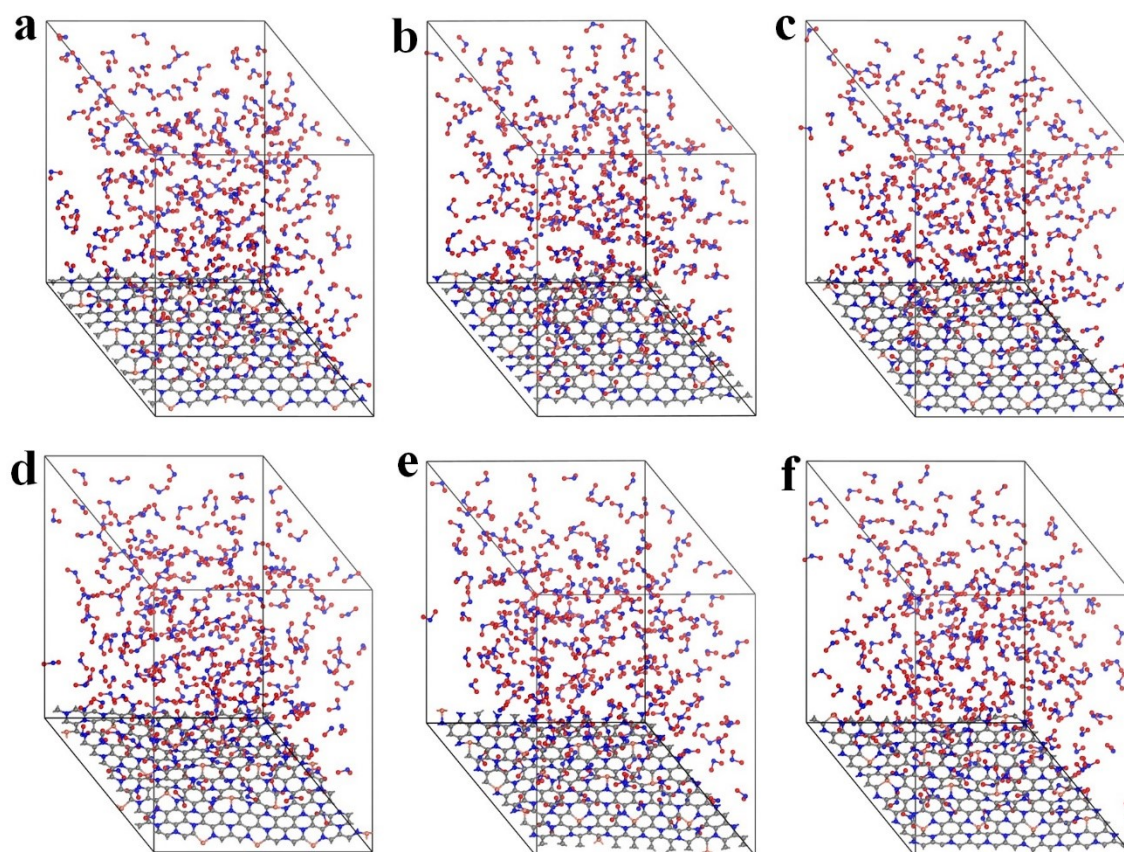


Figure S24. The stable configurations of NO₂ on the Cu-C₂N₁ at different temperatures. (a) 300 K, (b) 400 K, (c) 500 K, (d) 600 K, (e) 700 K, and (f) 800 K.

Table S1. The amount of charge transferred by the gas adsorbed.

Gas	Cu-C ₂ N ₁	Ag-C ₂ N ₁
C ₂ H ₄	-0.09	-0.07
H ₂ O	0.12	0.09
NO ₂	-0.48	-0.44
NH ₃	0.16	0.13
C ₂ H ₆	0.10	0.06
PF ₅	0.01	-0.91

Table S2. Diffusion coefficient of six gases on the Cu/Ag-C₂N₁ monolayer at 300 K.

Gas	Cu-C ₂ N ₁	Ag-C ₂ N ₁
C ₂ H ₄	4.89	5.78
H ₂ O	6.73	6.60
NO ₂	2.47	2.83
NH ₃	5.37	5.07
C ₂ H ₆	4.89	4.13
PF ₅	4.39	3.72

Table S3. Diffusion coefficients of NO₂ on the Cu/Ag-C₂N₁ at different temperatures.

T (K)	300	400	500	600	700	800
Cu-C ₂ N ₁	2.47	3.12	3.37	4.44	4.03	4.24
Ag-C ₂ N ₁	2.83	3.47	3.78	3.70	5.18	-

Table S4. The recovery time (s) of the gas on the Cu-C₂N₁.

T(K)	C ₂ H ₄	H ₂ O	NO ₂	NH ₃	C ₂ H ₆	PF ₅
273	4.3×10 ²⁴	2.0×10 ³	1.9×10 ⁵³	6.9×10 ¹³	11.6	3.6×10 ⁻⁹
300	2.2×10 ²¹	83.6	2.5×10 ⁴⁷	3.2×10 ¹¹	0.8	1.7×10 ⁻⁹
400	1.0×10 ¹³	2.0×10 ⁻²	3.6×10 ³²	4.3×10 ⁵	8.3×10 ⁻⁴	2.7×10 ⁻¹⁰
500	1.0×10 ⁸	2.3×10 ⁻⁴	4.4×10 ²³	1.3×10 ²	1.4×10 ⁻⁵	8.8×10 ⁻¹¹
600	4.7×10 ⁴	9.1×10 ⁻⁶	5.0×10 ¹⁷	0.6	8.8×10 ⁻⁷	4.2×10 ⁻¹¹
700	1.9×10 ²	9.3×10 ⁻⁷	2.9×10 ¹³	1.2×10 ⁻²	1.2×10 ⁻⁷	2.4×10 ⁻¹¹
800	3.2	1.7×10 ⁻⁷	1.9×10 ¹⁰	6.6×10 ⁻⁴	2.9×10 ⁻⁸	1.6×10 ⁻¹¹

Table S5. The recovery time (s) of the gas on the Ag-C₂N₁.

T(K)	C ₂ H ₄	H ₂ O	NO ₂	NH ₃	C ₂ H ₆	PF ₅
273	4.8×10 ¹⁶	49.4	1.9×10 ⁴⁸	1.4×10 ¹⁰	5.8×10 ⁻⁴	4.4×10 ⁵
300	1.3×10 ¹⁴	2.9	7.1×10 ⁴²	1.4×10 ⁸	9.5×10 ⁻⁵	1.1×10 ⁴
400	3.7×10 ⁷	2.2×10 ⁻³	1.4×10 ²⁹	1.3×10 ³	9.6×10 ⁻⁷	1.1
500	4.6×10 ³	3.0×10 ⁻⁵	8.1×10 ²⁰	1.2	6.1×10 ⁻⁸	4.3×10 ⁻³
600	11.2	1.7×10 ⁻⁶	2.7×10 ¹⁵	1.2×10 ⁻²	9.7×10 ⁻⁹	1.1×10 ⁻⁴
700	0.2	2.2×10 ⁻⁷	3.2×10 ¹¹	4.3×10 ⁻⁴	2.6×10 ⁻⁹	7.6×10 ⁻⁶

References

- [1] B. Delley, From molecules to solids with the DMol³ approach, *The Journal of chemical physics*, 113 (2000) 7756-7764.
- [2] J.P. Perdew, K. Burke, M. Ernzerhof, Generalized Gradient Approximation Made Simple, *Physical review letters*, 77 (1996) 3865-3868.
- [3] J.P. Perdew, Y. Wang, Accurate and simple analytic representation of the electron-gas correlation energy, *Physical review. B, Condensed matter*, 45 (1992) 13244-13249.
- [4] S. Grimme, Semiempirical GGA-type density functional constructed with a long-range dispersion correction, *Journal of computational chemistry*, 27 (2006) 1787-1799.
- [5] R.S. Mulliken, Electronic Population Analysis on LCAO–MO Molecular Wave Functions. I, *The Journal of chemical physics*, 23 (1955) 1833-1840.
- [6] L. Tao, J. Huang, X. Yin, Q. Wang, Z. Li, G. Wang, B. Cui, Adsorption Kinetics of CO₂ on a Reconstructed Calcite Surface: An Experiment-Simulation Collaborative Method, *Energy & Fuels*, 33 (2019) 8946-8953.